Uplink Spectral Efficiency Analysis of In-Building Distributed Antenna Systems

Temitope Alade, Huiling Zhu, *Member, IEEE,* and Jiangzhou Wang, *Senior Member, IEEE* .

***Abstract*—Providing high data rate wireless transmissions has been difficult in indoor environments, particularly in multi-floor buildings. One way to achieve high data rate wireless transmissions is to reduce the radio transmission distance between the transmitter and the receiver by using distributed antenna systems (DASs) and employing frequency reuse. However, due to the reuse of the limited available spectrum, co-channel interference can severely degrade system capacity. In this paper, the uplink spectral efficiency of an in-building DAS with frequency reuse is studied, where remote antenna units (RAUs) deployed on each floor throughout the building are connected to a central unit (CU) where received signals are processed. The impact of co-channel interference on system performance is investigated by using a propagation channel model derived from multi-floor, in-building measurement results. The proposed scheme exploits the penetration loss of the signal through the floors, resulting in frequency reuse in spatially separated floors, which increases system spectral efficiency and also reduces co-channel interference. A comparative analysis with conventional co-located antenna deployment at the floor center is provided. Location based RAU selection and deployment options are investigated. System performance is evaluated in terms of location-specific spectral efficiency for a range of potential mobile terminal (MT) locations and various in-building propagation characteristics.**

***Index Terms*—Wireless communications, spectral efficiency, distributed antenna system, frequency reuse, co-channel interference, multi-floor in-building propagation, Nakagami fading.**

I. Introduction

DUE to the increasing penetration of smartphones and tablet-type devices, the demand for indoor wireless mobile communications continues to increase. More than 80% of mobile traffic in existing mobile cellular networks originates from or terminate inside buildings [1]. However, penetration losses and complex indoor environments make delivering high data rate wireless transmissions inside buildings a tough challenge, particularly in high-rise residential and office buildings, airports, shopping malls, and other indoor environments where concentrations of mobile users can be extremely high. Moreover, penetration losses are more prominent at higher frequencies. As new multimedia services and high data rate application intensifies, providing high quality indoor voice and data services becomes increasingly important.

The distributed antenna system (DAS) has become a promising solution for next generation wireless systems because of its advantages of reduced access distance, extended coverage, increased capacity and data rates [2]. With DAS, multiple remote antenna units (RAUs) are geographically distributed and connected to a central unit (CU) via optical fibre or coaxial cable. DAS thus reduces path loss, transmit power, and cochannel interference, thereby improving system performance, particularly for those mobile terminals (MTs) near the edge of a cell. Prior work has established the benefits of DAS for improving coverage [3], reducing outage on the uplink [4], reducing outage on the downlink [5], and enhancing capacity in [6]. Results in [7] show that with the same antenna density, DAS outperforms the colocated antenna system (CAS) in terms of average and outage spectral efficiency. In [8], a thorough comparison of DAS and microcellular systems was presented, which theoretically proved that DAS with frequency reuse outperforms the microcellular system in spectral efficiency per sector, and cell edge spectral efficiency. Furthermore, cell edge performance analysis of the DAS was conducted in [9] and transmission schemes based on sum rate analysis were proposed in [10]. The application of the DAS in high speed trains has been proposed in [11]

However, most recent studies about DAS have focused on performance analysis in outdoor scenarios with cell sizes generally within thousands of meters. The results derived in outdoor DAS cannot be applied directly to three-dimensional (3D) in-building multi-floor propagation scenarios because of numerous interference sources from the upper and lower floors which are generally within a few meters. Furthermore, the variability of the environment can be vast for a short transmitter-receiver separation [12]. Hence, in cochannel deployments, interference modelling used in the conventional DAS is not suitable in building environments, and insightful researches are needed. Although the performance of the DAS and femto cell system was compared in an enterprise office building environment in [13], the channel modelling, interference problems and performance analysis in multi-floor in-building DAS are not well understood. Also in [14], the achievable rate of in-building DAS was evaluated for single user downlink transmission in high building environments. However, the luxury of no frequency reuse in each floor may be far from reality in large buildings. It is difficult to understand the effect of multiple cochannel floors in a multi-user uplink scenario with the results derived since the interfering sources in downlink transmission are RAU which are fixed in a location in the building. Furthermore, the impact of walls, RAU selection and deployment options, which can have a large impact on the performance of the overall communication system was not considered in [14]. To the best of the authors' knowledge, the uplink spectral efficiency achievable in a multi-floor multi-user

T. Alade, H.Zhu and J. Wang are with the are with School of Engineering and Digital Arts, University of Kent, Canterbury, CT2 7NT United Kingdom E-mails:{t.t.alade, h.zhu, j.z.wang}@kent.ac.uk
Manuscript received January 8, 2015; revised March 5, 2014.

indoor environment employing the DAS with frequency reuse has not been previously reported in literature.

This paper investigates the uplink spectral efficiency of an in-building DAS with multiple users, where RAUs are deployed on each floor throughout a multi-storey building. In contrast to the conventional DAS, the radio signal is confined to a smaller area, consequently, the path loss of the transmitted signal is much smaller, which implies that data rate is likely to be a great deal higher in the in-building DAS. However, the in-building DAS is likely to face a critical problem of interference if the same frequency channels are reused within the building. This is mainly because the propagation environment is considerably more compact and in-building architectural features are irregular. The achievable spectral efficiency of the DAS in this type of environment has received very little attention so far.

More specifically, our contributions are the following: We first explore the characteristics of the indoor propagation channel, and propose an indoor channel model which accounts for inter-floor interference caused by the effect of the building structure and its terrain. Frequency reuse among floors is considered, and the resulting impact on uplink spectral efficiency in a multi-user scenario is presented. We show a comparative analysis with conventional co-located antenna deployment at the floor center to justify the benefits of the DAS. The impact of antenna selection and RAU deployment strategy on system performance is also determined. Throughout the paper, the achievable uplink spectral efficiency is used as the metric to measure the performance of the wireless system.

The remainder of the paper is organised as follows. Details of the propagation and system models in high-rise buildings, which are used to analyse the performance of the system, are presented in Section II. The achievable spectral efficiency under a given BER constraint is analysed in Section III. Location based antenna selection via interference avoidance is discussed in Section IV. Section V provides a range of representative numerical results and conclusions are drawn in Section VI.

II. Channel and System Models

A. Channel model

The uplink transmission model in a multi-storey office building is shown in Fig. 1, where each floor represents a cell equipped with *N* evenly spaced, ceiling mounted RAUs which are located in the same position on every floor to serve a set of *U* uniformly located MTs across each floor. The RAUs are connected to a CU where received signals are constructively processed. All antennas are assumed to be omni-directional with an orientation that is freely adjustable. It is assumed that there are a total of *V* CUs, one on each floor (i.e. frequency is reused on every floor). Each floor has a similar construction with internal walls, and the same frequency band is assumed to be shared on each floor. For simple analysis, it is assumed that the floors are shaped as rectangular boxes with a common inter-floor spacing of *F* meters. Due to the limited form factor of MTs and for the convenience of analysis, we have assumed that each MT is equipped with a single antenna, however, we can expect MTs to be equipped with multiple antennas as well-this is indeed the case already in long term evolution advanced (LTE-Advanced) [15]. Each MT located across each floor at a height of v meters. The MT of interest, $u^{'}$, is located on the middle floor (reference floor) of the building. It is also assumed that there is a multi-storey building located a few meters away from the reference building. Similar assumptions have been reported in [12]. The same set of system parameters are assumed for comparative analysis with conventional co-located antenna deployment where all antennas are co-located at the center of the floor.

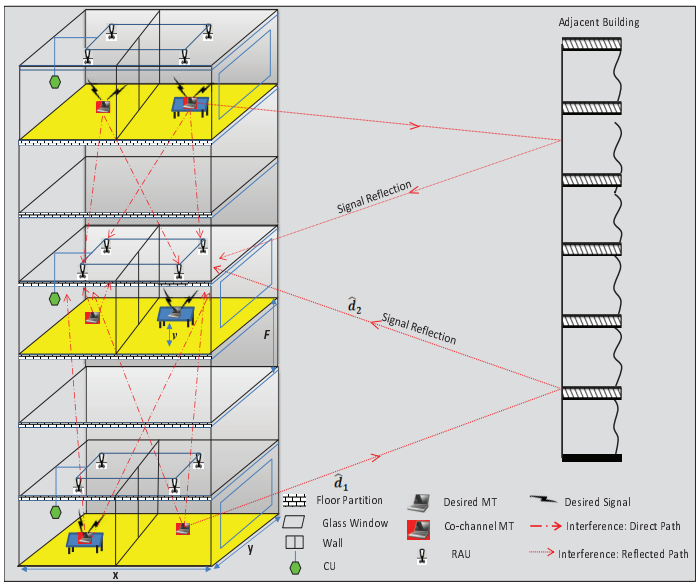

Fig. 1. An illustration of in-building DAS with frequency reuse

In radio propagation between floors of multi-storey buildings, experimental results have shown that there are two possible sources of interference. Depending on the structure of the building, and the location of the transmitter and the receiver, as shown in Fig.1, co-channel interference could emanate from [16]

1) direct signal transmission through the floor partitions, which may include multiple reflections between the walls, floors and ceilings;
2) transmissions that involve signal reflections and scattering from a nearby building that propagates back into the reference floor.

In this paper, specifically, the impact of co-channel interference from the direct and the reflected paths is studied. In this case, a RAU will receive a desired signal from a MT, and co-channel interfering signals from other MTs on the same or adjacent floors via direct signal penetration through the walls and floors, and reflections from a nearby building. For the sake of simplicity of the model, and focusing attention on getting considerable insight into the in-building DAS, it is assumed there is no interference originating from a neighbouring building.

The transmitted signal by MT-*u* to the *n*-th RAU can be

expressed as

$$\hat{x}_u(t) = Re\left[x_u(t)\right] = Re\left[\sqrt{P_s}\sum\nolimits_{i=-\infty}^{\infty} b_u\left[i\right]\rho_{T_s}(t-iT_s)e^{j2\pi f_c t}\right] \quad (1)$$

where $Re[x]$ represents the real part of x, $x_u(t)$ is the complex representation of the transmitted signal, P_s is the transmit power which is assumed to be the same for all MTs, $b_u\left[i\right]$ is the transmitted symbol (either real or complex) with $E[b_u]=0$ and $E[b_u \cdot b_u^*]=1$, where $*$ represents the complex conjugate. Note that b_u can be binary or non-binary. T_s represents the symbol duration, $\rho_{T_s}(t)$ is a pulse waveform defined as $\rho_{T_s}(t)=1$ for $0 \le t \le T_s$ and $\rho_{T_s}(t)=0$ otherwise and f_c is the carrier frequency.

The channel from MT-*u* to the *n*-th RAU on the reference floor is modelled as the sum of low pass equivalent impulse responses of the individual paths which can be expressed as

$$h_{u,n}(t) = h_{u,n}^{'}(t) + \hat{h}_{u,n}(t) \quad (2)$$

where $h_{u,n}^{'}(t)$ and $\hat{h}_{u,n}(t)$ are the impulse responses for the direct paths and the reflected paths from a neighbouring building, respectively. The complex low pass equivalent impulse response for $h_{u,n}^{'}(t)$ can be expressed as

$$h_{u,n}^{'}(t) = (d_{u,n})^{-\mu/2} \cdot \tilde{\varphi}_{u,n}^{l/2} \cdot \varphi_{u,n}^{k/2} \cdot \alpha_{u,n} \cdot e^{j\theta_{u,n}} \cdot \delta(t-\tau_{u,n}) \quad (3)$$

where $(d_{u,n})^{-\mu}$ is the distance dependent path loss when the signal propagates through the floors. $d_{u,n}$ is the distance between MT-*u* and the *n*-th RAU on the reference floor. μ is the path loss propagation exponent, and typically takes a value between 2 to 6 depending on the propagation condition (the variation can be attributed to the physical layout and type of building, as summarized in [17]). $\tilde{\varphi}_{u,n}$ and $\varphi_{u,n}$ are the penetration loss through a single wall and a single floor respectively, and l and k are the number of walls and floors in the transmission path respectively. The reported penetration loss for brick internal walls were found to be 3dB to 8dB per wall while floors made of concrete were found to be 10dB to 15dB per floor. Floors made of concrete over corrugated steel exhibit penetration loss as large as 26dB at 1700MHz (measurement values of penetration loss for different floor materials and wall types are summarized in [18]). It should be noted that, over the frequency range of interest (1.0-3.5 GHz) assumed in this study, the electromagnetic properties of typical materials encountered within buildings can be modelled as frequency independent [19]. In (3), $d_{u,n}$ is determined by the locations of the MT and the RAU. Assuming a (x, y, z) Cartesian coordinate system, let (x_u, y_u) denote the coordinate of the MT-*u*, and (x_n, y_n) represents the coordinate of the *n*-th RAU on the reference floor. Then the MT-RAU distance in 3D space is given by

$$d_{u,n} = \sqrt{(x_u - x_n)^2 + (y_u - y_n)^2 + [Fk + (v-F)]^2} \quad (4)$$

Note that the number of intervening floors between the desired MT and its target RAU on the reference floor is zero (i.e. $k=0$). $\alpha_{u,n}$, $\theta_{u,n}$ and $\tau_{u,n}$ in (3) are the channel fading coefficient, path phase, and path delay, respectively. It is assumed that $\alpha_{u,n}$, $\theta_{u,n}$ and $\tau_{u,n}$ are statistically independent. It is also assumed that $\theta_{u,n}$ and $\tau_{u,n}$ are uniformly distributed over $[0, 2\pi]$ and $[0, T_s]$, respectively. $\delta(t)$ denotes the Dirac delta function.

Similarly, the complex low pass equivalent impulse response of $\hat{h}_{u,n}(t)$ in (2) can be expressed as

$$\hat{h}_{u,n}(t) = \left(\hat{d}_{u,n}\right)^{-\hat{\mu}/2} \cdot \hat{\varphi}_{u,n}^{1/2} \cdot \ddot{\varphi}_{u,n} \cdot \tilde{\varphi}_{u,n}^{l/2} \cdot \hat{\alpha}_{u,n} \cdot e^{j\hat{\theta}_{u,n}} \cdot \delta(t-\hat{\tau}_{u,n}) \quad (5)$$

where $\hat{d}_{u,n}$ denotes the propagation distance between MT-*u* and the *n*-th RAU on the reference floor when the signal is reflected by a neighbouring building as illustrated in Fig. 1. $\hat{d}_{u,n}$ can be approximated by

$$\hat{d}_{u,n} = \hat{d}_1 + \hat{d}_2 \quad (6)$$

where $\hat{d}_1$ is the distance between MT-*u* and the neighbouring building, and $\hat{d}_2$ is the length of the reflected path from the neighbouring building to the *n*-th RAU on the reference floor. In (5), $\hat{\mu}$ is the path loss propagation exponent of the reflected path towards the neighbouring building (free space propagation is assumed, $\hat{\mu}=2$), $\hat{\varphi}_{u,n}$ is the reflection coefficient at the building surface and $\ddot{\varphi}_{u,n}$ is the transmission loss through the glass windows. Note that the reflection path experiences glass penetration loss twice. $\hat{\alpha}_{u,n}$, $\hat{\theta}_{u,n}$ and $\hat{\tau}_{u,n}$ are the channel fading coefficient, path phase and channel delay, respectively, for the reflected path. Since the line of sight (LOS) path of the reflected signal is blocked and scattered by the glass windows and the neighbouring building respectively, the fading distribution of $\hat{\alpha}_{u,n}$ can be approximated as Rayleigh distributed [16]. $\hat{\theta}_{u,n}$ and $\hat{\tau}_{u,n}$ tend to have the same distribution as $\theta_{u,n}$ and $\tau_{u,n}$ respectively. The small delay spread relative to long symbol interval is assumed as in modulation schemes like orthogonal frequency division multiplex (OFDM) [20]-[22]. Hence, the effect of intersymbol interference (ISI) on the system performance is negligible.

B. Received signal

The uplink received signal by the *n*-th RAU on the reference floor includes components from the desired MT-$u^{'}$, intra-floor interfering MT-$\hat{u}$, inter-floor interfering MT-*u* and channel noise. This can be represented by its complex low-pass equivalent as

$$\begin{aligned} r_{u,n}(t) &= x_{u'}(t) \otimes h_{u',n}(t) + \underbrace{\sum_{\hat{u}\in O, \hat{u}\neq u'} x_{\hat{u}}(t) \otimes h_{\hat{u},n}(t)}_{\text{intra-floor interference}} \\ &\quad + \underbrace{\sum_{u=1,u\neq u'}^{V} \sum_{u\in S} x_u(t) \otimes h_{u,n}(t)}_{\text{inter-floor interference}} + \eta_n(t) \\ &= D_s \cdot x_{u'}(t-\tau_{u',n}) + \sum_{\hat{u}\in O, \hat{u}\neq u'} (I_d + I_r) \cdot x_{\hat{u}}(t-\tau_{\hat{u},n}) \\ &\quad + \sum_{u=1,u\neq u'}^{V} \sum_{u\in S} (G_d + Q_r) \cdot x_u(t-\tau_{u,n}) + \eta_n(t) \end{aligned} \quad (7)$$

where the notation $\otimes$ denotes the convolution operation, O denotes the set of intra-floor interferers, S denotes the set of inter-floor interferers, $D_s = (d_{u',n})^{-\mu/2} \cdot \tilde{\varphi}_{u',n}^{l/2} \cdot \alpha_{u',n} \cdot e^{j\theta_{u',n}}$, $I_d = (d_{\hat{u},n})^{-\mu/2} \cdot \tilde{\varphi}_{\hat{u},n}^{l/2} \cdot \alpha_{\hat{u},n} \cdot e^{j\theta_{\hat{u},n}}$, $I_r = (\hat{d}_{\hat{u},n})^{-\hat{\mu}/2} \cdot \hat{\varphi}_{\hat{u},n}^{1/2} \cdot \ddot{\varphi}_{\hat{u},n} \cdot \tilde{\varphi}_{\hat{u},n}^{l/2} \cdot \hat{\alpha}_{\hat{u},n} \cdot e^{j\hat{\theta}_{\hat{u},n}}$, $G_d = (d_{u,n})^{-\mu/2} \cdot \tilde{\varphi}_{u,n}^{l/2} \cdot \varphi_{u,n}^{k/2} \cdot \alpha_{u,n} \cdot e^{j\theta_{u,n}}$, $Q_r = (\hat{d}_{u,n})^{-\mu/2} \cdot \hat{\varphi}_{u,n}^{1/2} \cdot \ddot{\varphi}_{u,n} \cdot \tilde{\varphi}_{u,n}^{l/2} \cdot \hat{\alpha}_{u,n} \cdot e^{j\hat{\theta}_{u,n}}$ and $\eta_n(t)$ is the additive white Gaussian noise (AWGN) at the *n*-th RAU, with zero mean and a double sided power spectral density $N_0/2$.

In [23], channel measurements were performed to determine channel characteristics in and around office and factory buildings where a LOS is present. The measurements showed that the channel follows a Nakagami-*m* fading distribution, where the received signal consists of several specular components plus several Rayleigh fading components. The Nakagami-*m* distribution provides a very good fit for measured data in a variety of fading environments. The envelop of the desired signal is modelled by Nakagami-*m* distribution. Hence, $\alpha_{u',n}^2$ is Gamma distributed with the probability distribution function (pdf) expressed as in [24]

$$p_{\alpha_{u',n}^2}(\alpha_{u',n}^2) = (\frac{m_n}{\Omega_n})^{m_n} \frac{(\alpha_{u',n}^2)^{m_n-1}}{\Gamma(m_n)} \exp(-\frac{m_n}{\Omega_n}\alpha_{u',n}^2), \quad \alpha_{u',n} \leq 0 \tag{8}$$

where $\Gamma(\cdot)$ is the Gamma function defined by $\Gamma(x) = \int_0^\infty t^{x-1}e^{-t}dt$, m_n is a parameter accounting for the fading severity and Ω_n is the average fading power of the received signal. The parameters Ω_n and m_n can be expressed as $\Omega_n = E[\alpha_{u',n}^2]$ and $m_n = \frac{\Omega_n^2}{E[(\alpha_{u',n}^2 - \Omega_n)^2]}, m_n \geq \frac{1}{2}$, respectively. It is assumed that interfering signals have no specular component due to intervening wall and floors; therefore, the envelop of the interfering signal is Rayleigh distributed with mean square $E[\alpha_{u,n}^2] = 1$. The pdf of the instantaneous interfering signal power in the Rayleigh fading channel can be obtained by letting $m_n = 1$.

Assuming the phase and the path delay are known at the receiver and the receiver has a perfect timing synchronisation with the MT-u' i.e., $\tau_{u',n} = 0$, the demodulated signal of MT-u' over one symbol period T_s is given by

$$\begin{aligned} Z_n &= Re\left\{\frac{1}{T_s}\int_0^{T_s} r_{u,n}(t) \cdot e^{-j2\pi f_c t} \cdot e^{-j\theta_{u',n}} \; dt\right\} \\ &= Re\left[S_n + \sum_{\hat{u}\in O, \hat{u}\neq u'} I_{u,n}^O + \sum_{u=1,u\neq u'}^{V} \sum_{u\in S} I_{u,n}^S\right] + \eta_n \end{aligned} \tag{9}$$

where S_n is the desired signal component received by the *n*-th RAU on the reference floor, expressed as

$$\begin{aligned} S_n &= \frac{1}{T_s}\int_0^{T_s} D_s \cdot x_{u'}(t) \cdot e^{-j\theta_{u',n}} \cdot e^{-j2\pi f_c t} dt \\ &= \sqrt{P_s} \cdot \left(d_{u',n}\right)^{-\mu/2} \cdot \tilde{\varphi}_{u',n}^{l/2} \cdot b_{u'} \cdot \alpha_{u',n} \end{aligned} \tag{10}$$

$I_{u,n}^O$ is the intra-floor interfering signal component expressed as

$$\begin{aligned} I_{u,n}^O &= \frac{1}{T_s}\int_0^{T_s} \left(I_d \cdot x_{\hat{u}}(t-\tau_{\hat{u},n}) \cdot e^{-j\theta_{\hat{u},n}} \right. \\ &\qquad \left. + I_r \cdot x_{\hat{u}}(t-\hat{\tau}_{\hat{u},n}) \cdot e^{-j\hat{\theta}_{\hat{u},n}}\right) dt \\ &= \frac{\hat{I}_d}{T_s}\left(\int_0^{\tau_{\hat{u},n}} b_{\hat{u}}[i] + \int_{\tau_{\hat{u},n}}^{T_s} b_{\hat{u}}[i+1]\right) dt \\ &\quad + \frac{\hat{I}_r}{T_s}\left(\int_0^{\hat{\tau}_{\hat{u},n}} b_{\hat{u}}[i] + \int_{\hat{\tau}_{\hat{u},n}}^{T_s} b_{\hat{u}}[i+1]\right) dt \\ &= \frac{\hat{I}_d}{T_s}\left[b_{\hat{u}}[i] \cdot (\tau_{\hat{u},n}) + b_{\hat{u}}[i+1] \cdot (T_s - \tau_{\hat{u},n})\right] \\ &\quad + \frac{\hat{I}_r}{T_s}\left[b_{\hat{u}}[i] \cdot (\hat{\tau}_{\hat{u},n}) + b_{\hat{u}}[i+1] \cdot (T_s - \hat{\tau}_{\hat{u},n})\right] \end{aligned} \tag{11}$$

where $\hat{I}_d = (d_{\hat{u},n})^{-\mu/2} \cdot \tilde{\varphi}_{\hat{u},n}^{l/2} \cdot \alpha_{\hat{u},n} \cdot e^{j(\theta_{\hat{u},n} - \theta_{u',n})}$, $I_r = (\hat{d}_{\hat{u},n})^{-\hat{\mu}/2} \cdot \hat{\varphi}_{\hat{u},n}^{1/2} \cdot \ddot{\varphi}_{\hat{u},n} \cdot \tilde{\varphi}_{\hat{u},n}^{l/2} \cdot \hat{\alpha}_{\hat{u},n} \cdot e^{j(\hat{\theta}_{\hat{u},n} - \theta_{u',n})}$. $b_{\hat{u}}[i]$ and $b_{\hat{u}}[i+1]$ are the previous and current symbols transmitted by MT-$\hat{u}$ within $[0, T_s]$ respectively.

$I_{u,n}^S$ is the inter-floor interfering signal component expressed as

$$\begin{aligned} I_{u,n}^S &= \frac{1}{T_s}\int_0^{T_s} \left(G_d \cdot x_u(t-\tau_{u,n}) \cdot e^{-j\theta_{u,n}} \right. \\ &\qquad \left. + Q_r \cdot x_u(t-\hat{\tau}_{u,n}) \cdot e^{-j\hat{\theta}_{u,n}}\right) dt \\ &= \frac{\hat{G}_d}{T_s}\left(\int_0^{\tau_{u,n}} b_u[i] + \int_{\tau_{u,n}}^{T_s} b_u[i+1]\right) dt \\ &\quad + \frac{\hat{Q}_r}{T_s}\left(\int_0^{\hat{\tau}_{u,n}} b_u[i] + \int_{\hat{\tau}_{u,n}}^{T_s} b_u[i+1]\right) dt \\ &= \frac{\hat{G}_d}{T_s}\left[b_u[i] \cdot (\tau_{u,n}) + b_u[i+1] \cdot (T_s - \tau_{u,n})\right] \\ &\quad + \frac{\hat{Q}_r}{T_s}\left[b_u[i] \cdot (\hat{\tau}_{u,n}) + b_u[i+1] \cdot (T_s - \hat{\tau}_{u,n})\right] \end{aligned} \tag{12}$$

where $\hat{G_d} = (d_{u,n})^{-\mu/2} \cdot \tilde{\varphi}_{u,n}^{l/2} \cdot \varphi_{u,n}^{k/2} \cdot \alpha_{u,n} \cdot e^{j(\theta_{u,n} - \theta_{u',n})}$ and $\hat{Q_r} = (\hat{d}_{u,n})^{-\hat{\mu}/2} \cdot \hat{\varphi}_{u,n}^{1/2} \cdot \ddot{\varphi}_{u,n} \cdot \tilde{\varphi}_{u,n}^{l/2} \cdot \hat{\alpha}_{u,n} \cdot e^{j(\hat{\theta}_{u,n} - \theta_{u',n})}$. $b_u[i]$ and $b_u[i+1]$ are the previous and current symbols transmitted by the MT-*u* within $[0, T_s]$ respectively. The total co-channel interference term received by the *n*-th RAU on the reference floor, denoted by I_n, is written as

$$I_n = \sum_{\hat{u}\in O, \hat{u}\neq u'} I_{u,n}^O + \sum_{u=1,u\neq u'}^{V} \sum_{u\in S} I_{u,n}^S \tag{13}$$

Note that interfering signals are independent of each other, accordingly, the total co-channel interference term I_n is a zero mean Gaussian distributed random variable. The expectation of I_n as a sum of complex Gaussian random variables can be easily derived as $E[I_n] = 0$ and the variance denoted by $\sigma_{I_n}^2$

is derived in Appendix A as

$$\sigma_{I_n}^2 = \frac{P_s}{3}\sum_{\hat{u}\in O,\hat{u}\neq u'}[(d_{\hat{u},n})^{-\mu}\tilde{\varphi}_{\hat{u},n}^{l} + (\hat{d}_{\hat{u},n})^{-\hat{\mu}}\hat{\varphi}_{\hat{u},n}\ddot{\varphi}_{\hat{u},n}^{2}\tilde{\varphi}_{\hat{u},n}^{l}] + \frac{P_s}{3}\sum_{u=1,u\neq u'}^{V}\sum_{u\in S}[(d_{u,n})^{-\mu}\tilde{\varphi}_{u,n}^{l}\varphi_{u,n}^{k} + (\hat{d}_{u,n})^{-\hat{\mu}}\hat{\varphi}_{u,n}\ddot{\varphi}_{u,n}^{2}\tilde{\varphi}_{u,n}^{l}] \quad (14)$$

In (9), η_n is the noise component with zero mean and a variance of $\sigma_\eta^2 = N_0/(2T_s)$, which is assumed to be equal for all RAUs.

C. Minimum mean square error combining with successive interference cancellation

At the receiver of the CU, the minimum mean square error combining (MMSEC) is applied, where the received signal by the *n*-th RAU, given in (9), is multiplied by a controllable weight in order to achieve spatial diversity. In the MMSEC spatial diversity scheme, the combiner output used for the detection is a linear combination of the weighted signals of all the RAUs on the reference floor. To get better performance, the MMSEC is followed by a successive interference cancellation where the order of decoding MT is based on decreasing SINR [25]. In MMSE-SIC, the input for detecting MT-u is the received signal after subtracting the signal component of the MT-1 through MT-$(u-1)$. The MMSEC decision variable for detecting the desired signal on the reference floor is given by

$$Z_0 = \sum_{n=1}^{N} W_n \cdot Z_n = \sum_{n=1}^{N}\left(W_n \cdot S_n + W_n \cdot \sum_{u=1,u\neq u'}^{V} I_{u,n} + W_n \cdot \eta_n\right) \quad (15)$$

where W_n is the optimum weight which maximizes the signal-to-interference-plus-noise ratio (SINR). In the presence of co-channel interference, MMSEC spatial diversity is used not only to combat the fading of the desired signal (as with maximal ratio combining (MRC), which is the optimum combiner in a noise only system) but also to suppress the power of the interfering signals at the receiver. However, when there is no interference, MMSEC maximizes the output signal-to-noise ratio (SNR) and its performance is then equivalent to that of MRC. The optimum weight, W_n, is expressed as [25]

$$W_n = \frac{\alpha_{u'n}}{\rho_n}(d_{u',n})^{-\mu/2}\tilde{\varphi}_{u',n}^{l/2} \quad (16)$$

where $\alpha_{u'n}$ is the channel fading coefficient of the desired signal and ρ_n is the variance of the interfering signal plus background noise at the *n*-th RAU on the reference floor, written as

$$\rho_n = E\left[I_n \cdot I_n^*\right] + \sigma_\eta^2 = \sigma_{I_n}^2 + \sigma_\eta^2 \quad (17)$$

Substituting $E\left[I_n \cdot I_n^*\right]$ with (A4) as derived in Appendix A into (17), ρ_n is rewritten as

$$\rho_n = \frac{P_s}{3}\sum_{\hat{u}\in O,\hat{u}\neq u'}[\hat{I}] + \frac{P_s}{3}\sum_{u=1,u\neq u'}^{V}\sum_{u\in S}[\tilde{I}] + \sigma_\eta^2 \quad (18)$$

where $\hat{I} = (d_{\hat{u},n})^{-\mu}\tilde{\varphi}_{\hat{u},n}^{l} + (\hat{d}_{\hat{u},n})^{-\hat{\mu}}\hat{\varphi}_{\hat{u},n}\ddot{\varphi}_{\hat{u},n}^{2}\tilde{\varphi}_{\hat{u},n}^{l}$ and $\tilde{I} = (d_{u,n})^{-\mu}\tilde{\varphi}_{u,n}^{l}\varphi_{u,n}^{k} + (\hat{d}_{u,n})^{-\hat{\mu}}\hat{\varphi}_{u,n}\ddot{\varphi}_{u,n}^{2}\tilde{\varphi}_{u,n}^{l}$.
Therefore the optimum weight, W_n, is given by

$$W_n = \frac{\alpha_{u',n}(d_{u',n})^{-\mu/2}\tilde{\varphi}_{u',n}^{l/2}}{\frac{P_s}{3}\sum_{\hat{u}\in O,\hat{u}\neq u'}[\hat{I}] + \frac{P_s}{3}\sum_{u=1,u\neq u'}^{V}\sum_{u\in S}[\tilde{I}] + \sigma_\eta^2} \quad (19)$$

Correspondingly, the instantaneous SINR is written as

$$\begin{aligned}\gamma &= \frac{\left(\sum_{n=1}^{N} W_n S_n\right)^2}{\sum_{n=1}^{N} W_n^2\sigma_{I_n}^2 + \sum_{n=1}^{N} W_n^2\sigma_\eta^2} = \frac{\left(\sum_{n=1}^{N} W_n S_n\right)^2}{\sum_{n=1}^{N} W_n^2\left(\sigma_{I_n}^2 + \sigma_\eta^2\right)} \\ &= \frac{\left(\sum_{n=1}^{N}\frac{\sqrt{P_s}}{\rho_n}\cdot(d_{u',n})^{-\mu}\tilde{\varphi}_{u',n}^{l}\alpha_{u',n}^{2}\right)^2}{\sum_{n=1}^{N}\left(\frac{\alpha_{u',n}^{2}(d_{u',n})^{-\mu}\tilde{\varphi}_{u',n}^{l}}{\rho_n^2}\right)\cdot\rho_n} \\ &= \sum_{n=1}^{N}\frac{P_s(d_{u',n})^{-\mu}\tilde{\varphi}_{u',n}^{l}}{\rho_n}\alpha_{u',n}^{2}\end{aligned} \quad (20)$$

Since $\alpha_{u'n}^2$ is Gamma distributed, the pdf of the instantaneous SINR, γ, in (20), for arbitrary values of the Nakagami fading parameters is then obtained as [26]

$$P_\gamma(\gamma) = \frac{1}{\pi}\int_0^\infty \frac{\cos\left[\sum_{n=1}^{N} m_n\tan^{-1}\left(\frac{t}{\beta_n}\right) - t\gamma\right]}{\prod_{n=1}^{N}\left(1+\left(\frac{t}{\beta_n}\right)^2\right)^{m_n/2}}dt \quad (21)$$

where $\beta_n = m_n/\bar{\gamma}_n$. $\bar{\gamma}_n$ is the average SINR per RAU given by

$$\begin{aligned}\bar{\gamma}_n &= \frac{P_s\cdot(d_{u',n})^{-\mu}\tilde{\varphi}_{u',n}^{l}}{\frac{P_s}{3}\sum_{\hat{u}\in O,\hat{u}\neq u'}[\hat{I}] + \frac{P_s}{3}\sum_{u=1,u\neq u'}^{V}\sum_{u\in S}[\tilde{I}] + \frac{N_0}{2T_s}}\cdot\Omega_n \\ &= \frac{\frac{2E_s}{N_0}\cdot(d_{u',n})^{-\mu}\tilde{\varphi}_{u',n}^{l}}{\frac{2}{3}\cdot\frac{E_s}{N_0}\left(\sum_{\hat{u}\in O,\hat{u}\neq u'}[\hat{I}] + \sum_{u=1,u\neq u'}^{V}\sum_{u\in S}[\tilde{I}]\right) + 1}\cdot\Omega_n\end{aligned} \quad (22)$$

where $\frac{E_s}{N_0}$ is the transmit symbol energy-to -noise density ratio at the MT transmitter location and E_s is expressed as

$$E_s = P_s\cdot T_s \quad (23)$$

III. Achievable Spectral Efficiency

The adaptive multi-level quadrature amplitude modulation (MQAM) which dynamically determines the modulation level based on the received SINR is applied to maximize spectral efficiency while keeping the bit error rate (BER) under a target value. This is important since applications require a certain maximum BER. During a good channel condition, a higher modulation level is used, while during a poor channel condition, a lower modulation level is used. The relationship

between BER and SINR, γ, under a certain modulation level $M_{\hat{j}} = 2^{\hat{j}}$ for MQAM can be approximated as [27]

$$\hat{P}_e(\gamma) = \frac{1}{5}\exp\left[\frac{-3\gamma}{2(2^{\hat{j}}-1)}\right] \tag{24}$$

where $\hat{j}$ (an even number) is the number of bits per symbol. Given a target instantaneous BER equal to $\hat{P}_0$, the SINR region boundaries (or adaptive modulator switching thresholds) $\gamma_{\hat{j}}$ for switching across the modulation level can be solved from the inverse of (23)

$$\gamma_{\hat{j}} = -\frac{2}{3}(2^{\hat{j}}-1)\ln(5\hat{P}_0); \quad \hat{j} = 0, 2, 4, \cdots, J \tag{25}$$

where J is the maximum number of bits per symbol. The average spectral efficiency with unit of bits per second per Hertz, is defined as the sum of the data rates, $\log_2(M_{\hat{j}}) = \hat{j}$, weighted by the probability that the $\hat{j}$-th modulation constellation is assigned to MT-$u^{'}$. This can be expressed as

$$T_u = \sum_{\hat{j}=1}^{J} \log_2(M_{\hat{j}}) \int_{\gamma_{\hat{j}}}^{\gamma_{\hat{j}+1}} P_\gamma(\gamma) d\gamma \tag{26}$$

where the values of $\gamma_{\hat{j}}$ and $\gamma_{\hat{j}+1}$ are obtained respectively from (24) for a given $\hat{P}_0$. Note that γ_{J+1} is assumed infinite. By substituting (20) into (25), interchanging the order of integration and simplifying trigonometric identities, T_u is rewritten as

$$T_u = \sum_{\hat{j}=1}^{J} \log_2(M_{\hat{j}}) \times \frac{1}{\pi}\int_0^\infty -\frac{\sin(B_1(t) - t\gamma_{\hat{j}+1}) - \sin(B_1(t) - t\gamma_{\hat{j}})}{tB_2(t)} dt \tag{27}$$

where $B_1 = \sum_{n=1}^{N} m_n \cdot \tan^{-1}(\frac{t}{\beta_n})$ and $B_2 = \prod_{n=1}^{N}(1 + (\frac{t}{\beta_n})^2)^{m_n/2}$

IV. Location-Specific Antenna Selection

In this section, a location-specific antenna selection strategy, where a set of $N^{'}$ strongest RAUs out of N available RAUs is selected for combining, is investigated in the in-building DAS.

In uplink transmission, the system performance is sensitive not only on the closeness of the desired MT to its RAU, but also to the location of the co-channel MTs within the building. This is due to the range of possible geometric arrangements of MTs. With reference to Fig. 2, the path loss of the interfering MT can even be much smaller than that of the desired MT in some locations across the floor. Accordingly, the system performance is evaluated to show the effect of MT locations for various geometric arrangements and two RAU deployment options shown in Figs. 2(a) and (b), single line configuration, and square configuration respectively. It is also important to note that due to large transmission path loss or the effect of strong co-channel interfering signals, some RAUs may have insignificant contributions to the total received signal. Such RAUs could be discarded in order to avoid interference and save considerable amount of the receiver's signal processing.

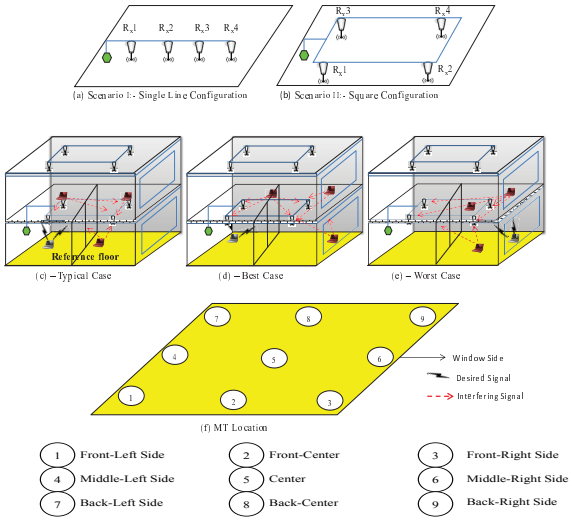

Fig. 2. RAU locations and MT geometrical arrangements

In conventional two dimensional (2D) outdoor cellular DAS networks, the path loss-based antenna selection is utilised, where the RAUs closest to the MT would be selected for combining [5]. However, selecting such RAUs in uplink transmission of 3D inter-floor communication may not enhance the system performance if a co-channel MT is located on a floor directly above (or below) the selected RAU. Therefore, a selection strategy which determines the appropriate RAUs to select for combining based on specific location of MTs is suggested as follows. If both the desired and co-channel MTs are located at the center of the floor, all N RAUs can be selected for combining however, when both MTs are located at the side of the floor, selecting just two RAUs may in fact be sufficient. This way, only RAUs with significant SINRs are selected for combining before taking detection decision. This finding is verified in Section V through Fig. 9, where the achievable spectral efficiency is shown as a function of the parameter SNR for different values of N' at specific locations of MTs.

V. Numerical Results

In this section, a range of results for illustrating the achievable spectral efficiency of the exemplified DAS in multi-storey buildings is presented.

In order to present numerical results, the analytic formulas derived in Sections II, III and IV are evaluated for the building structure shown in Fig. 1 in an uplink scenario. Unless specified otherwise, the following assumptions are made.

- A 7-story building is considered.
- Inter-floor spacing F is 4m.
- The floor dimension (x, y) is 40m x 40m.
- 2 MTs are evenly located across each floor at height v of 1m.
- 4 RAUs are deployed on the ceiling of each floor.
- 4 antennas are co-located at the center of each floor for the conventional centralized deployment i.e. $(x_n, y_n) = (0, 0)$ for any antenna.

- Path loss exponent μ is 2.5.
- Path loss exponent of the reflected path $\hat{\mu}$ is 2.0
- Penetration loss $\tilde{\varphi}$ is 6.5dB per wall and φ is 13dB per floor, which is consistent with the results reported in [18] for penetration loss of about 5 to 8dB for brick walls and 10 to 15dB for concrete floors.
- Reflection loss $\hat{\varphi}$ at the surface of the neighbouring building and penetration loss $\ddot{\varphi}$ through two sets of glass windows is 18dB, which is consistent with observations made by [16].
- The distance between the reference and the adjacent building $\hat{d}_{u,n}$ is 10m.
- Nakagami fading values $\{m_1, m_2, m_3, m_4\} = \{1.8, 1.5, 1.0, 1.0\}$.
- E_s/N_0 is 30dB.
- The target BER $\hat{P}_0$ is 10^{-3}.
- The achievable spectral efficiency is with respect to the desired MT located on the reference floor.

Figs. 3(a) and (b) compare the achievable spectral efficiency between the system with conventional deployment with co-located antenna and the in-building DAS. In order to make a fair comparison, 4 antenna elements are assumed for both systems and total transmitted power is the same for both cases. It can be clearly seen from these figures that the in-building DAS outperforms the conventional system with co-located antennas thanks to the reduction in access distance. Unlike the conventional system, the in-building DAS shows four peaks at the location of each RAU as shown in Fig. 3(a), thus providing a more uniform coverage. RAUs in floor regions close to the same floor co-channel MT suffer from much higher interference thus leading to degraded performance in that location. The performance of both systems is sensitive to the locations of MTs but the conventional system is more sensitive to localised effects. As illustrated in Fig. 3(b), high spectral efficiency is generally localised to (relatively) small regions directly above base-stations antennas located at the floor center. MTs located at the floor boundary suffer from much higher interference and path loss than those at the cell center - cell edge problem. The average spectral efficiency

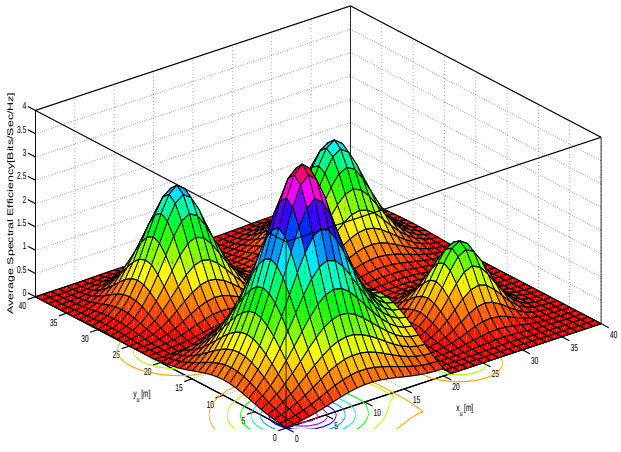

(a) In-building DAS

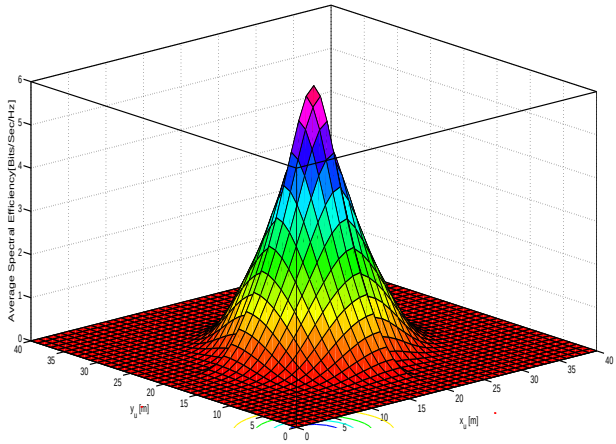

(b) Co-located antenna deployment

Fig. 3. Achievable spectral efficiency comparison between in-building DAS and co-located antenna deployment

over the entire floor (i.e. 2.4 bits/sec/Hz for in-building DAS and 1.3 bits/sec/Hz for the conventional system) shows that In-building DAS outclasses the conventional system and it is worth the change. It is also expected that the performance gap between the two systems becomes more pronounced as the number of intra-floor MT reduces, leading to a much higher spectral efficiency across many floor regions for the in-building DAS.

Figs. 4(a) and (b) presents the location specific performance over a range of possible MT location with the consideration of two RAU deployment scenarios, the single line configuration and the square configuration as shown in Fig. 2(a) and (b). Intuitively, the system performance is considerably better in Senario II than in Scenario I, especially at the floor sides owing to the short distances between the desired MT and the RAUs in this configuration. For example, for Scenario II, it is observed that 25.9% of location combinations show high spectral efficiency values greater than 2.0 bits/sec/Hz, a value close to the best case, while for Scenario I, high spectral efficiency values greater than 2.0 bits/sec/Hz occur only when the desired MT is located at the middle-left and middle-right sides of the floor. However, it is important to note that the square configuration is more sensitive to MT locations. It can be seen from Fig. 4(a) that 8.9% of MT location combinations show low spectral efficiency close to the worst case value, while for single line configuation in Fig. 4(b), only 4.1% of MT location combinations show spectral efficiency lower than 2.5 bits/sec/Hz, The average of these spectral efficiencies over a large number of uniformly distributed MT locations, shows that RAU deployment according to Scenario II is preferable. This result is significant, as it indicates that the RAU position is important in the design of in-building wireless system for high data rates. Scenario II will be assumed from hereon.

The advantage of the above analysis is that, it does not only take into account the performance of the system associated with fading and the effect of co-channel interference, but also takes into account the likelihood of MTs being in certain

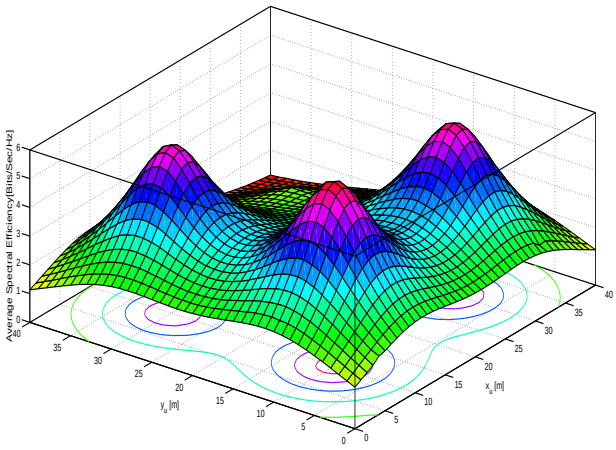

(a) Co-channel MT located at the back-right side of the floor, a position corresponding to one RAU location

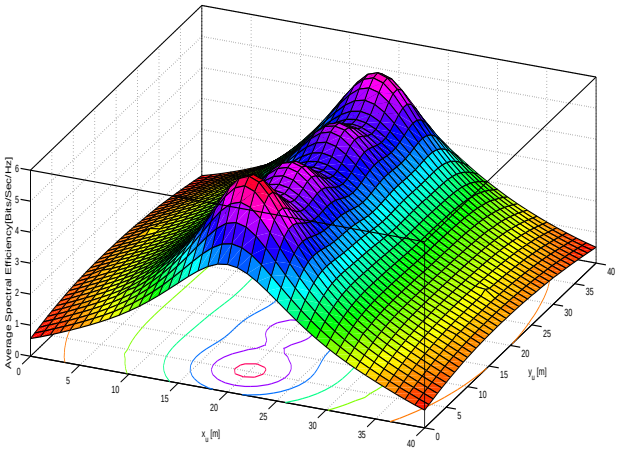

(b) Co-channel MT located at the floor center (Scenario I)

Fig. 4. Location-specific achievable spectral efficiency

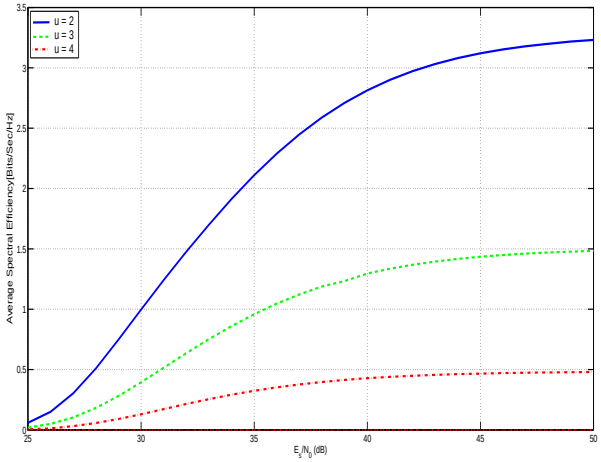

Fig. 5. Effect of the number of MTs per floor

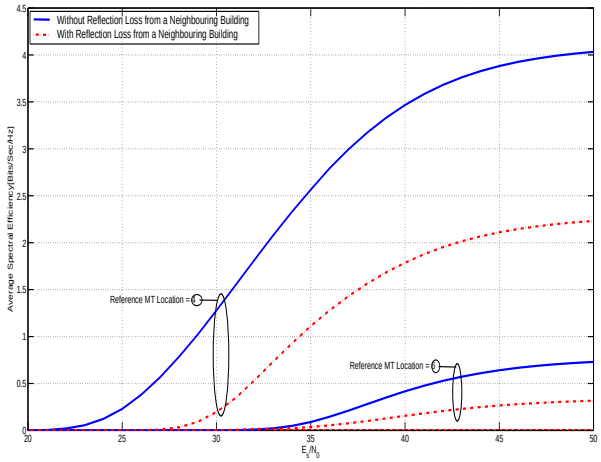

Fig. 6. Effect of reflection loss on achievable spectral efficiency

locations across the floor. Thus, based on the above analysis of location-specific spectral efficiency, efficient resource allocation schemes through intelligent channel reuse in a multi-user environment can be proposed. For example, an MT can be assigned the same channel if a co-channel MT is not vertically aligned at the same location on immediate adjacent floors of the building.

Figs. 5 illustrates the achievable spectral efficiency with respect to the number of users per floor. The results show that the system performance reduces as the number of co-channel users/user density increases. For the two user case, the spectral efficiency increases linearly with SNR, but as more users are introduced, the distance between same floor MTs reduces and more RAUs suffer from high co-channel interference. Interference dominates the performance and the achievable spectral efficiency saturates and tends to be flat at high SNR regions.

Fig. 6 shows the achievable spectral efficiency for a scenario without reflection loss from a neighbouring building compared with a scenario with reflection loss from a neighbouring building. The desired MT is located at the middle-right side of the floor, a position which is strongly affected by severe reflection from the neighbouring building, i.e. position ⑥ in Fig. 2(f). It is observed from the figure that when reflection is not considered, an optimistic system performance is clearly evident especially at high SNR region. In general, it is found for both cases that the main impairment to achievable spectral efficiency is co-channel interfering signals received from direct signal transmission through the floors. However, when there is reflection from a neighbouring building, co-channel interference from reflection contributes towards the received interference power. It can be seen that ignoring reflection makes the result too optimistic. The co-channel interference from the neighbouring building should be considered in the worst case. The total co-channel interference makes the achievable spectral efficiency to gradually become flat when SNR is higher than about 40dB. When SNR is smaller than 30dB, the noise dominates the interference, and it can be seen from this figure that performance for both cases are almost indistinguishable. However, the combined effect of the interference from the direct and reflected paths on the performance dominates noise at high SNR values. It is

apparent that the system achieves a better performance when the desired MT is located at the left side of the floor than at the right side. This is because, at the right side, desired MT is closer to the neighbouring building, where the effect of reflection from the neighbouring building is most dominant. This lowers the received SINR and thereby reduces the system performance.

Figs. 7(a) and (b) shows the achievable spectral efficiency for different floor and wall types respectively. Depending on the composition of the floors and walls inside the building, a significant reduction in the total received signal to interference power is due to wall and floor penetration losses. If floors are made of corrugated steel panels of about 20dB penetration loss for example, an evaluation of the potential spectral efficiency can be made. It can be seen from Fig. 7 that the spectral efficiency achievable increases with increasing penetration loss, owing to greater isolation from co-channel MTs. High inter-floor/wall isolation ensures high SINR and high spectral efficiency across the floor. Moreover, it is evident from Fig. 7(a) that when SNR = 30dB, the achievable spectral efficiency increases linearly at first, and saturates when penetration loss is larger than 16dB.

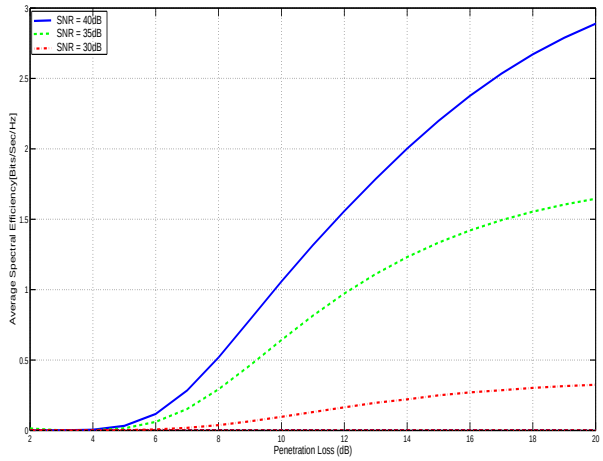

(a) Effect of floor penetration loss on achievable spectral efficiency

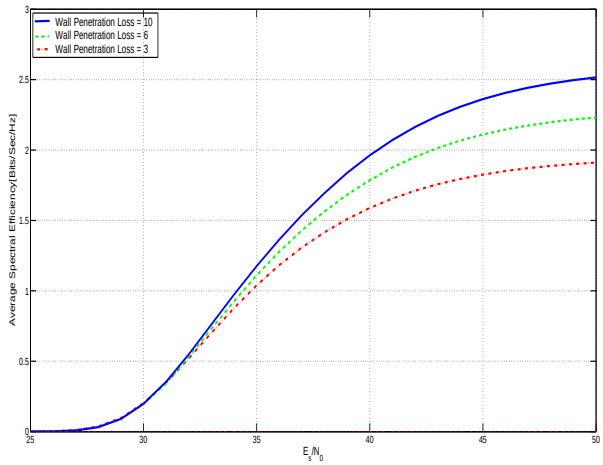

(b) Effect of wall penetration loss on achievable spectral efficiency

Fig. 7. Achievable spectral efficiency versus penetration loss

The reason is that the effect of channel noise on achievable spectral efficiency dominates the co-channel interference effect. Thus, the effect of co-channel interference becomes negligible with increasing penetration loss values. On the other hand, the system benefits from the increase in SNR, e.g. when SNR = 35dB, the achievable spectral efficiency grows linearly and then tends to be flat as penetration loss increases to about 20dB due to the dominant effect of co-channel interference for very large SNR values. Similar effect is observed for wall penetration loss in Fig. 7(b). Although the desired signal power is reduced due to the walls, the interfering signal of the same floor MT also decreases but not eliminated.

Fig. 8 depicts the achievable spectral efficiency as a function of SNR when the strongest RAUs are selected. It is observed that when the reference MT is located on the left side of the floor, the system performance for $N^{'} = 4$, $N^{'} = 3$ and $N^{'} = 2$ is the same. R_x1 and R_x3 are the useful diversity branches that can appreciably contribute to the received signal without any redundancy. R_x2 or R_x4 could be discarded due to strong co-channel interference and the wall penetration loss.The discarded RAU represents no loss in appreciable received signal. This way, the requirement for phase and amplitude estimation on each RAU can be reduced. However, when MTs are positioned at the center of the floor, all RAUs should be selected.

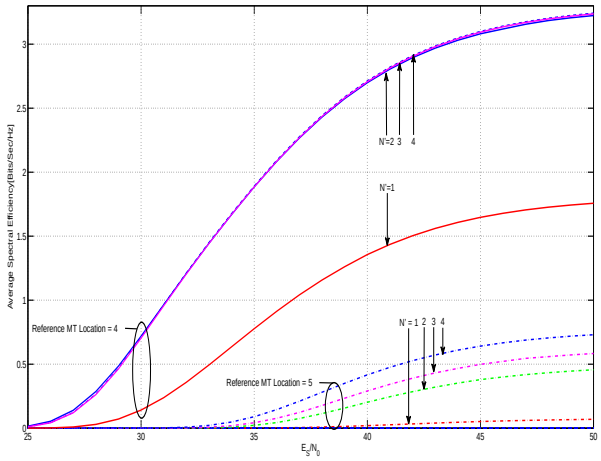

Fig. 8. Achievable spectral efficiency at specific MT locations when the strongest RAUs are selected

Fig. 9 show the results for scenarios with different path loss exponent. In reality, the path loss exponent can vary for different building layouts. It is observed that the higher the pathloss exponent, the lower the system performance. This is due to increased path loss. Although the path loss for the interfering MTs is increased, the path loss of the desired MT is equally increased as μ increases. Thus, similar trends are observed for the given values of μ. The spectral efficiency increases linearly with SNR and saturates at high SNR regions due to the impact of co-channel interference which dominates the system performance.

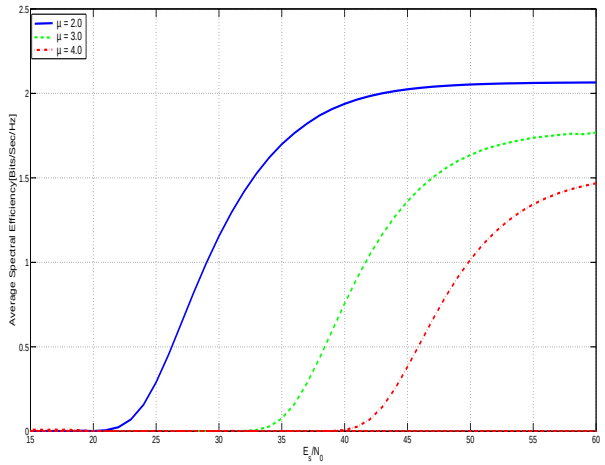

Fig. 9. Achievable spectral efficiency versus pathloss exponent

VI. Conclusion

In-building DAS can provide high data rates for indoor MTs. By considering vertically located co-channel MTs, the achievable spectral efficiency in a multi-storey building is studied, by using a propagation channel model derived from multi-floor, in-building measurement results. The following conclusions have been drawn:

1) The in-building DAS outperforms the conventional system with co-located antennas for indoor wireless communications. The highest spectral efficiency values are shown in floor regions closer to the desired RAU, if a co-channel MT is not vertically aligned above the RAU location, while regions directly above/below the interfering MTs are found to have the lowest spectral efficiency values compared to rest of the floor. The worst case spectral efficiency occurs when the desired MT and the co-channel MT are both located close to the window.
2) The square configuration for RAU deployment (Scenario II) outperforms the single line configuration (Scenario I) especially at the floor sides/boundaries. However, low spectral efficiency near the worst case value is not likely to occur in the single line configuration, due to greater isolation from co-channel MTs. Consequently, RAU location can have a major impact on system performance in high-rise buildings and as such is an important design consideration and should be determined to maximize spectral efficiency.
3) By selecting RAUs for combining based on maximum received instantaneous power at specific locations of MTs across the floor, which also reduces the effect of co-channel interference, it is found that RAUs with weak signal can be eliminated. The discarded RAUs represent no loss in appreciable spectral efficiency.
4) Penetration loss has a significant impact on achievable spectral efficiency especially when SNR is large.
5) The impact of reflection from a neighbouring building cannot be disregarded when the reference MT is located in floor regions close to the neighbouring building.

Appendix A
Derivation of Variance of Co-Channel Interference in (14)

In this appendix, the variance of the total co-channel interference term in (14) is derived. From (13)

$$I_n = \sum_{\hat{u}\in O,\hat{u}\neq u'} I^O_{u,n} + \sum_{u=1,u\neq u'}^{V}\sum_{u\in S} I^S_{u,n} \tag{A1}$$

where $I^O_{u,n}$ and $I^S_{u,n}$is given in (11) and (12) respectively, then I_n is rewritten as

$$\begin{aligned} I_n = &\sum_{\hat{u}\in O,\hat{u}\neq u'} \left(\frac{\hat{I}_d}{T_s}\left[b_{\hat{u}}[i]\cdot(\tau_{\hat{u},n}) + b_{\hat{u}}[i+1]\cdot(T_s-\tau_{\hat{u},n})\right] \right. \\ &\left. + \frac{\hat{I}_r}{T_s}\left[b_{\hat{u}}[i]\cdot(\hat{\tau}_{\hat{u},n}) + b_{\hat{u}}[i+1]\cdot(T_s-\hat{\tau}_{\hat{u},n})\right]\right) \\ &+ \sum_{u=1,u\neq u'}^{V}\sum_{u\in S}\left(\frac{\hat{G}_d}{T_s}\left[b_u[i]\cdot(\tau_{u,n}) + b_u[i+1]\cdot(T_s-\tau_{u,n})\right] \right. \\ &\left. + \frac{\hat{Q}_r}{T_s}\left[b_u[i]\cdot(\hat{\tau}_{u,n}) + b_u[i+1]\cdot(T_s-\hat{\tau}_{u,n})\right]\right) \end{aligned} \tag{A2}$$

The variance can be expressed as

$$\begin{aligned} \sigma^2_{I_n} &= E\left[I_n\cdot I_n^*\right] \\ &= E\left\{ \sum_{\hat{u}\in O,\hat{u}\neq u'} \left(\left[\frac{\sqrt{P_s}\cdot(d_{\hat{u},n})^{-\mu/2}\cdot\tilde{\varphi}^{l/2}_{\hat{u},n}\cdot\alpha_{\hat{u},n}}{T_s}\right] \right.\right. \\ &\quad \cdot\left[b_{\hat{u}}[i]\cdot(\tau_{\hat{u},n}) + b_{\hat{u}}[i+1]\cdot(T_s-\tau_{\hat{u},n})\right] \\ &\quad + \left[\frac{\sqrt{P_s}\cdot(\hat{d}_{\hat{u},n})^{-\hat{\mu}/2}\cdot\hat{\varphi}^{1/2}_{\hat{u},n}\cdot\ddot{\varphi}_{\hat{u},n}\cdot\tilde{\varphi}^{l/2}_{\hat{u},n}\cdot\hat{\alpha}_{\hat{u},n}}{T_s}\right] \\ &\quad \left.\cdot\left[b_{\hat{u}}[i]\cdot(\hat{\tau}_{\hat{u},n}) + b_{\hat{u}}[i+1]\cdot(T_s-\hat{\tau}_{\hat{u},n})\right]\right) \\ &\quad + \sum_{u=1,u\neq u'}^{V}\sum_{u\in S}\left(\left[\frac{\sqrt{P_s}\cdot(d_{u,n})^{-\mu/2}\cdot\tilde{\varphi}^{l/2}_{u,n}\cdot\varphi^{k/2}_{u,n}\cdot\alpha_{u,n}}{T_s}\right] \right. \\ &\quad \cdot\left[b_u[i]\cdot(\tau_{u,n}) + b_u[i+1]\cdot(T_s-\tau_{u,n})\right] \\ &\quad + \left[\frac{\sqrt{P_s}\cdot(\hat{d}_{u,n})^{-\mu/2}\cdot\hat{\varphi}^{1/2}_{u,n}\cdot\ddot{\varphi}_{u,n}\cdot\tilde{\varphi}^{l/2}_{u,n}\cdot\hat{\alpha}_{u,n}}{T_s}\right] \\ &\quad \left.\left.\cdot\left[b_u[i]\cdot(\hat{\tau}_{u,n}) + b_u[i+1]\cdot(T_s-\hat{\tau}_{u,n})\right]\right)\right\}^2 \end{aligned} \tag{A3}$$

Since $E\left[\alpha^2_{u,n}\right]=1$, $E[b_u]=0$, $E[b_u\cdot b_u^*]=1$ and $E\left[\tau^2_{u,n}\right] = E\left[(T_s-\tau_{u,n})^2\right] = \frac{T_s^2}{3}$, and similarly, $E\left[\hat{\alpha}^2_{u,n}\right]=1$, and $E\left[\hat{\tau}^2_{u,n}\right] = E\left[(T_s-\hat{\tau}_{u,n})^2\right] = \frac{T_s^2}{3}$, the real and the imaginary parts of I_n have the same variance expressed as

$$\begin{aligned} \sigma^2_{I_n} = &\frac{P_s}{3}\sum_{\hat{u}\in O,\hat{u}\neq u'}\left[(d_{\hat{u},n})^{-\mu}\tilde{\varphi}^l_{\hat{u},n} + (\hat{d}_{\hat{u},n})^{-\hat{\mu}}\hat{\varphi}_{\hat{u},n}\ddot{\varphi}^2_{\hat{u},n}\tilde{\varphi}^l_{\hat{u},n}\right] \\ &+ \frac{P_s}{3}\sum_{u=1,u\neq u'}^{V}\sum_{u\in S}\left[(d_{u,n})^{-\mu}\tilde{\varphi}^l_{u,n}\varphi^k_{u,n}\right. \\ &\left. + (\hat{d}_{u,n})^{-\hat{\mu}}\hat{\varphi}_{u,n}\ddot{\varphi}^2_{u,n}\tilde{\varphi}^l_{u,n}\right] \end{aligned} \tag{A4}$$

Equation (A4) leads to the variance of the total co-channel interference term in (14) at *n*-th RAU on the reference floor.

REFERENCES

[1] P. Cerwall, S. Bergqvist, "Ericsson Traffic and Market Data Report [R]". November, 2011 www.ericsson.com

[2] J. Park, E. Song, and W. Sung, "Capacity analysis for distributed antenna system using cooperative transmission schemes in fading channels," *IEEE Trans. Wireless Commun*., vol. vol.8, no. 2, pp. 586-592, Feb. 2009.

[3] J. Zhang and J. G. Andrews, "Distributed antenna systems with randomness," *IEEE Trans. Wireless Commun*., vol. 7, no. 9, pp. 3636-3646, Sept. 2008.

[4] L. Dai, S. Zhou, and Y. Yao, "Capacity analysis in CDMA distributed antenna systems," *IEEE Trans. Wireless Commun*., vol. 4, no. 6, pp. 2613-2620, Nov. 2005.

[5] Y. Liu, J. Liu, W. Guo, and H. Xu, "Outage probability and bit-error rate analysis of distributed antenna systems in multicell environment," *IET Commun*., pp. 791-798, Aug. 2013.

[6] R. Heath, S. Peters, Y. Wang and J. Zhang, "A current perspective on distributed antenna systems for the downlink of cellular systems," *IEEE Commun. Mag*., vol.51, no. 4, pp. 161-167, Apl. 2013.

[7] L. Dai, "A comparative study on uplink sum capacity with co-located and distributed Antennas," *IEEE J. Select Areas Commun*., vol. 29, no. 6, pp. 1200-1213, June 2011.

[8] H. Zhu, "Performance comparison between distributed antenna and microcellular systems," *IEEE J. Select Areas Commun*., vol. 29, no. 6, pp. 1151-1163, June 2011.

[9] X. You, D. Wang, P. Zhu and B. Sheng, "Cell edge performance of cellular mobile systems," *IEEE J. Select Areas Commun*., vol. 29, no. 6, pp. 1139-1150, June 2011.

[10] H. Kim, S.R. Lee, K.J. Lee, and I. Lee, "Transmission schemes based on sum rate analysis in distributed antenna systems," *IEEE Trans. Wireless Commun*., vol. 11, pp. 1201-1209, Mar. 2012.

[11] J. Wang, H. Zhu, and N. Gomes, "Distributed antenna systems for mobile communications in high speed trains," *IEEE J. Select Areas Commun*., vol. 30, pp. 675-683, May 2012.

[12] T. Alade, H. Zhu and H. Osman, "Performance evaluation of DAS for interfloor wireless communications," *Proc. IEEE ICC*., pp. 4788-4792, 2012.

[13] L. Zhen, T. Sorensen, J. Wigard, and P. Mogensen, "DAS, uncoordinated femto and joint scheduling systems for in-building wireless solutions," *Proc. IEEE VTC*., pp. 1-5, 2011.

[14] H. Osman, H. Zhu, D. Toumpakaris, and J. Wang, "Achievable rate evaluation of in-building distributed antenna systems," *IEEE Trans. Wireless Commun*., vol. 12, no. 7, pp. 3510-35215, July 2013.

[15] H. Holma and A. Toskala, LTE Advanced: "3GPP Solution for IMTAdvanced," 1st ed. Wiley, 2012.

[16] C. M. Austin, M. J. Neve, G. B. Rowe and R. J. Pirkl, "Modelling the effects of nearby buildings on inter-floor radio wave propagation," *IEEE Trans. Antennas and Propag*., vol. 57. no. 7, pp. 2155-2161, July 2009.

[17] T. K. Sarkar, Z. Ji, K. Kim, A. Medouri, and M. Salazar-Palma, "A survey of various propagation models for mobile communication," *IEEE Antennas Propag. Mag*., vol. 45, no. 3, pp. 5182, June 2003.

[18] S.Y. Seidel and T. S. Rappaport, "914 MHz path loss prediction models for indoor wireless communications in multifloored buildings," *IEEE Trans. Antennas and Propag.*, AP-40, (2), pp. 207-217, 1992.

[19] Recom. ITU-R P.1238-7, "Propagation data and prediction methods for the planning of indoor radio communication systems and radio local area networks in the frequency range 900 MHz to 100 GHz," 2012.

[20] H. Zhu and J. Wang, "Chunk-based resource allocation in OFDMA systems - part I: chunk allocation," *IEEE Trans. Commun*., vol. 57, no. 9, pp. 2734-2744, Sept 2009.

[21] H. Zhu, "Radio Resource Allocation for OFDMA Systems in High Speed Environments," *IEEE J. Select Areas Commun*., vol. 30, pp. 748-759, May 2012.

[22] H. Zhu and J. Wang, "Chunk-based resource allocation in OFDMA systems - part II: Joint chunk allocation, power allocation and bit allocation" *IEEE Trans. Commun*., vol. 60, no. 2, pp. 499-509, Feb. 2012.

[23] N. Goodman and K. Kathleen, "The impact of antenna directivity on the small-scale fading in indoor environments," *IEEE Trans. Antennas and Propag.*, vol. 54, no. 12, pp. 3771-3777, Dec. 2006.

[24] J. Wang and J. Chen, "Performance of wideband CDMA with complex spreading and imperfect channel estimation," *IEEE J. Select. Areas Commun*, vol. 19, no. 1, pp. 152-163, Jan. 2001.

[25] V. Aalo and J. Zhang, "Average error probability of optimum combining with a co-channel interferer in nakagami fading," *IEEE Wireless Commun. and Netw. Conf*., vol. 1, pp. 376-381, July 2000.

[26] G. Efthymoglou and V. Aalo, "Performance of RAKE receivers in Nakagami fading channel with arbitrary fading parameters," *IEEE Electronic Lett.*, vol.31, No.18, pp. 1610-1612, Aug. 1995.

[27] M. S. Alouini and A. J. Goldsmith, "Adaptive modulation over Nakagami fading channels," *Wireless Pers. Commun*., vol. 13, pp. 119-143, May 2000.

Temitope Alade received his B.Sc. degree in Computer Science from the University of Ilorin, M.Sc. degree in Mobile Computing from the University of Bradford and Ph.D. degree in Electronic Engineering from the University of Kent. He is currently a Lecturer in Mobile Communications at the School of Engineering and Digital Arts, University of Kent, Canterbury, United Kingdom. His research interests are in the areas of mobile/wireless communication systems and, in particular, methods of designing reliable high capacity networks, radiowave propagation and modelling in cellular/microcellular/indoor environments, in-building DAS and MIMO systems, interference mitigation and cancellation, system planning, deployment, and performance analysis. Dr. Alade was a member of the organising committee and web chair for IEEE WCNC 2013 in Shanghai.

Huiling Zhu (M'04) received the B.S degree from Xidian Univeristy, Xi'an, China, and the Ph.D. degree from Tsinghua University, Beijing, China. She is currently a Lecturer (Assistant Professor) in the School of Engineering and Digital Arts, University of Kent, Canterbury, United Kingdom. Her research interests are in the area of broadband wireless mobile communications, covering topics such as radio resource management, MIMO, cooperative communications, distributed antenna systems, device to device communications, and small cells and heterogeneous networks. She has participated in a number of European and industrial projects in these topics. She has served as the Publication Chair of IEEE WCNC2013 and is the Operation Chair of IEEE ICC2015. She is current an editor of IEEE Transactions on Vehicular Technology.

Jiangzhou Wang is currently the Chair of Telecommunications and Head of Broadband and Wireless Communications Research Group with the School of Engineering and Digital Arts, University of Kent, United Kingdom. He has published over 200 papers in international journals and conferences in the areas of wireless mobile communications and has written/edited three books. He received the Best Paper Award from IEEE Globecom2012. His research interests include wireless mobile communications, massive MIMO and small-cell technologies, device to device communications in cellular networks, distributed antenna systems, and cooperative communications. Professor Wang is a Fellow of the IET and was an IEEE Distinguished Lecturer from 1/2013 to 12/2014. He serves/served as an Editor or Guest Editor for a number of international journals, such as IEEE Transactions on Communications and IEEE Journal on Selected Areas in Communications. He was the Technical Program Chair of the IEEE WCNC2013 in Shanghai and the Executive Chair of the IEEE ICC2015 in London.